On stochastic dynamic analysis and assessment of bistable structures

Xianbo Sun[a], Yahui Zhang[a*], David Kennedy[b]

[a] *State Key Laboratory of Structural Analysis for Industrial Equipment, Department of Engineering Mechanics, International Center for Computational Mechanics, Dalian University of Technology, Dalian 116023, PR China*

[b] *School of Engineering, Cardiff University, Cardiff CF24 3AA, Wales, UK*

Corresponding author:

Dr. Y. H. Zhang

State Key Laboratory of Structural Analysis for Industrial Equipment, Department of Engineering Mechanics, Faculty of Vehicle Engineering and Mechanics, Dalian University of Technology, Dalian 116023, PR China

Email: zhangyh@dlut.edu.cn

Tel: +86 411 84708393

Fax: +86 411 84708393

Abstract

This paper investigates some basic issues on the stochastic dynamic analysis and assessment of bistable structures from an applications perspective, illustrated with a classical spring-mass-rod structure. A complete Lagrangian-description-based Monte Carlo simulation and an Eulerian-description-based Fokker-Planck equation analysis are implemented respectively to capture the evolution process of the physical response probability density function, with special focus on the dynamics under the statistical steady state condition. A comparison of these two methods outlines their capabilities. As a representative example, quantitative counting and statistical analysis of the number and amplitudes of snapping-through of the structure indicate that physical quantities for structural assessment may show certain statistical regularities under the statistical steady state condition, which can be utilized efficiently to reduce the efforts of structural assessment without loss of precision.

Key words: *Bistable structures; Monte Carlo simulation; Fokker-Planck equation; Statistical steady state; Probability density evolution*

1 Introduction

Multistable dynamic systems play an important role in a variety of disciplines, such as physics, chemistry and neurosciences [1-4]. In structural analysis and design, bistable structures are currently receiving much attention, especially with respect to their dynamic characteristics. For example, utilizing the post-buckling strength [5-7] of slender/thin-walled components may lead to more effective designs for high-performance aerospace structures. To this end, the dynamic analysis and assessment of buckled components working in extreme, combined environments must be carefully investigated [8-13]. In the last decade, it has been found that bistable structures produce noticeable improvement in the efficiency of mechanical energy absorption compared with traditional monostable structures [14]. They have also proved to be promising in the design of broadband vibration energy harvesters as self-powered sources for portable devices or wireless sensor network systems, and the reader is referred to [15-19] for more details. For other emerging topics, e.g. unidirectional wave propagation characteristics, or applications, e.g. for morphing

designs, see [20-26] and a more comprehensive review in [27]. In conclusion, utilization of bistable structures broadens the scope for design, and is now an active research field in which the dynamic analysis and related assessment of bistable structures are of crucial importance and certainly will promote further applications.

Bistable structures exhibit strong nonlinear behaviors. The deterministic dynamic response of bistable structures can be obtained straightforwardly by a direct time integration of the kinematic differential equations [9,10,13]. When the loads are not completely ascertained, which is usually the case for practical engineering problems, the amount of computation required is often very large and needs to be reduced without significant loss of precision. Generally, two kinds of methodologies, namely Lagrangian-description-based methods which take the physical response as basic unknowns, and Eulerian-description-based methods which take the physical response probability density function (PDF) as basic unknowns, can be used to govern the behaviors of a stochastic dynamic system [4,28,29]. As is known, the former is the main methodology adopted in dynamic analysis of structures. The governing equations of bistable structures derived in this framework are nonlinear stochastic/random differential equations (SDEs [28] or RDEs [29], also referred to in this paper as governing equations in physical space) which usually need to be solved by Monte Carlo simulation (MCS). Most investigations involving stochastic dynamics of bistable structures have taken this approach [6,8,12]. Researches on Brownian motion in the early 20th century indicate that assuming the response has the Markovian property (this can be verified in structure analysis, as illustrated in Ref. [28]), the governing equations of stochastic dynamic systems can be expressed in an Eulerian framework with the physical response PDF as basic unknowns, e.g. the Kolmogorov equations among others [4,30].

It is noted that in this case the inherent continuity of the physical response is neglected and cannot be recovered from the PDF. The forward Kolmogorov equations, i.e. Fokker-Planck equations (FPE) [4,28-31] are commonly used and can be seen in some investigations involving stochastic dynamics of bistable structures [11,18,19].

The present paper focuses on the stochastic dynamic analysis and assessment of bistable structures from an applications perspective through a simple spring-mass-rod structure (SMRS). The following two topics are primarily involved.

1) Comparison of Lagrangian-description-based methods and Eulerian-description-based methods. It is noted that an ergodicity hypothesis [32,33] for the physical response of the bistable structures is usually made without proof in the related engineering researches [8,12,14]. Consequently, time averaging of a single sample path with remarkably reduced amount of computation replaces necessary ensemble averaging, but the statistics obtained may be unreliable since the response process of a structure may be not ergodic, and the statistical evolutionary regularities of the physical response are not revealed by this approach. On the other hand, when FPEs are adopted [19], the finite element method (FEM) or finite differential method (FDM) are usually needed to solve these equations numerically since their analytical solutions can rarely been found [4,28-31,34-36]. In this paper, a complete MCS using ensemble averaging and a FPE analysis using FEM are implemented to capture the evolution process of the physical response PDF. The ensemble of sample paths given by MCS is converted into an Eulerian framework. Comprehensive discussions follow the comparison between the results obtained by these two methods.

2) Statistical regularities of physical quantities for structural assessment under

the statistical steady state condition. It is known that the physical response PDF of a structure excited by stationary random loads tends to be time-independent after a transient evolution process [4,28-31,34-36], where the ultimate PDF is actually the steady state solution of the corresponding FPE. The term "statistical steady state" is used in this paper to refer to the final statistically stationary dynamic state. A primary concern is the existence of statistical regularities of the physical quantities for structural assessment under the statistical steady state condition. As a representative example, in view of the movement characteristics of bistable structures, and in analogy with the handling of stress/strain cycles in the rainflow counting method for fatigue life assessment [37-39], the statistics of the number and amplitudes of snapping-through of the structure are investigated. Numerical results demonstrate the deduced statistical regularities under the statistical steady state condition. Subsequently, the utilization of such statistical regularities to dramatically reduce the efforts of structural assessment without loss of precision is illustrated.

The rest of this paper is organized as follows. Section 2 introduces the SMRS investigated and the bistable mechanisms revealed therein for general structures. Similar models can also be found in [40]. The governing equations in physical space and the corresponding FPE are also given. For ease of presentation, the excitation is assumed to be Gaussian white noise. Section 3 presents feasible procedures for applying such equations to obtain the evolution process of the physical response PDF. In Section 4, the statistical regularities of the number and amplitudes of snapping-through are deduced rationally. Numerical examples, verifications and discussions are given in Section 5. Section 6 summarizes the paper.

2 Structural bistability and governing equations

2.1 SMRS and bistable mechanisms

A single-degree-of-freedom SMRS is shown in Fig. 1. The spring-mass system k_s-m_s offers stiffness and inertia in the horizontal direction, while k_a-m_a mainly offers stiffness and inertia in the transverse direction. The mass of the springs and rods are neglected, along with gravity, and the rods are assumed to be rigid. This structure has the primary mechanical characteristics of common engineering components, e.g. beams, plates and shells, and thus it is thought to be able to reveal the mechanical behaviors of such components.

Suppose $\Theta = \theta_0$ is a static equilibrium position of the structure, with restoring forces F_s^0 and F_a^0 in the springs k_s and k_a, respectively. F_s^0 and F_a^0 satisfy the static equilibrium condition

$$F_a^0 = 2F_s^0 \tan\theta_0 \tag{1}$$

On this basis, restoring forces in the springs k_s and k_a with a general deformation Θ can be expressed as

$$\begin{aligned} &F_s = F_s^0 + k_s\Delta_s,\ \ F_a = F_a^0 + k_a\Delta_a \\ &\Delta_s = 2L(\cos\theta_0 - \cos\Theta),\ \ \Delta_a = L(\sin\theta_0 - \sin\Theta) \end{aligned} \tag{2}$$

where Δ_s and Δ_a are the deformation increments of the springs. Taking $\Theta = \theta_0$ as the zero-potential position, the elastic potential energy is given as

$$\begin{aligned} V(\Theta) &= \int_0^{\Delta_s} (F_s^0 + k_s\Delta_s)\,\mathrm{d}\Delta_s + \int_0^{\Delta_a} (F_a^0 + k_a\Delta_a)\,\mathrm{d}\Delta_a \\ &= 2F_s^0 L[(\cos\theta_0 - \cos\Theta) + \tan\theta_0\,(\sin\theta_0 - \sin\Theta)] \\ &\quad +2k_s L^2(\cos\theta_0 - \cos\Theta)^2 + \frac{1}{2}k_a L^2(\sin\theta_0 - \sin\Theta)^2 \end{aligned} \tag{3}$$

where Eq. (1) is utilized to eliminate F_a^0.

The monostability or bistability of the structure are determined by the number of minima of the function $V(\Theta)$, i.e. the number of stable static equilibrium positions of the structure. Setting $k_a = k_s = 15\text{N/m}$ and $L = 1\text{m}$, $V(\Theta)$ is then absolutely decided by the parameters F_s^0 and θ_0. Thus, the distribution of monostability and bistability of the structure over the parameter space F_s^0-θ_0 in the meaningful range $\Theta \in (-\pi/2, \pi/2)$ can be numerically detected, as shown in Fig. 2(a).

It is seen in Fig. 2(a) that parameters (F_s^0, θ_0) in the black area lead to structures which have only one stable static equilibrium position, a representative elastic potential energy function of which is shown as the black line in Fig. 2(b). These structures usually show moderate restoring force $(\partial V/\partial \Theta)$ and stiffness $(\partial^2 V/\partial \Theta^2)$ properties and vibrate in a reciprocating manner around the single static equilibrium position $\Theta = \theta_0$. Parameters (F_s^0, θ_0) in the red area lead to bistable structures with two stable static equilibrium positions. A representative elastic potential energy function is shown as the red line in Fig. 2(b), in which a potential barrier $\Theta = \theta_0$ separates two potential wells around the stable static equilibrium positions $\Theta = \theta_{s,1}$ and $\Theta = \theta_{s,2}$. Bistable structures usually exhibit two forms of motion, i.e. the intra-well response in a single well and the cross-well response that passes across the potential barrier from one potential well to the other. The cross-well response should be noted because it is generally accompanied by a sudden switching of motion statuses and encourages structural damages [8-13]. On the other hand, however, it is noted that bistable structures find distinct advantages in structural design by virtue of this drastic response characteristic [14-19]. Parameters (F_s^0, θ_0) in the gray area lead to unstable structures which are not considered in this paper.

In Fig. 2(a), points on the line $F_s^0 = 0$ correspond to a series of unloaded SMRSs (from Eq. (1) $F_a^0 = 0$), and the values of θ_0 are interpreted as the curvatures of engineering components. It can be observed that the line $F_s^0 = 0$ intersects with the red area, which actually indicates the curvature of an engineering component may render it to be bistable. Besides, if these SMRSs are statically loaded in the horizontal direction through the spring k_s, then the corresponding equilibrium paths can be given as in Fig. 3, where $\theta_0 = 0$rad and $\theta_0 = 1$rad are taken as representative examples.

In Fig. 3, the boundaries 1 and 2 are the same as in Fig. 2(a). Static equilibrium paths of a flat SMRS ($\theta_0 = 0$rad) and a curved SMRS ($\theta_0 = 1$rad) are marked as blue and red, respectively. A solid line means the equilibrium path is stable, and a dashed line means it is unstable. In fact, it is easy to show that Fig. 3 presents the nonlinear buckling paths of the SMRSs, and boundary 1 reveals the buckling loads. As the horizontal load decreases, the original monostable SMRSs are changed to become bistable at the crossing point P_1, and soon become unstable at the crossing point P_2 accompanied by the disappearance of stable equilibrium paths. As a result, buckling would also lead to bistable engineering components.

2.2 Governing equations in physical space

As shown in Fig. 1, consider a Gaussian white noise $W(t)$ with strength D [18] acting on the mass m_a. The kinetic energy and the external potential energy can be expressed as

$$T = \frac{1}{2} m_a L^2 \dot{\theta}^2 + \frac{1}{2} m_s \dot{\Delta}_s^2, \qquad \mathcal{W} = W \Delta_a \tag{4}$$

where $\dot{(\cdot)}$ denotes a partial derivative with respect to time. The Lagrange function and the Rayleigh dissipation function are defined as

$$\mathcal{L} = T - V - \mathcal{W}, \qquad \mathcal{F} = \frac{1}{2} c\dot{\Theta}^2 \tag{5}$$

where c is the viscous damping coefficient. Substituting Eq. (5) into Lagrange's equations gives

$$\frac{\mathrm{d}}{\mathrm{d}t}\left(\frac{\partial \mathcal{L}}{\partial \dot{\Theta}}\right) - \frac{\partial \mathcal{L}}{\partial \Theta} + \frac{\partial \mathcal{F}}{\partial \dot{\Theta}} = 0 \tag{6}$$

The governing equations in physical space are obtained as

$$\begin{aligned}(m_a \sec\Theta + 4m_s \sin\Theta \tan\Theta)L\ddot{\Theta} + 4m_s L \sin\Theta\, \dot{\Theta}^2 + c/L \sec\Theta\, \dot{\Theta} \\ + 2(F_s^0 + 2k_s L\cos\theta_0)\tan\Theta + (k_a - 4k_s)L\sin\Theta \\ - 2F_s^0 \tan\theta_0 - k_a L \sin\theta_0 = W\end{aligned} \tag{7}$$

Defining a state vector $\boldsymbol{X} = [X_1, X_2]^{\mathrm{T}} = \left[\Theta, \dot{\Theta}\right]^{\mathrm{T}}$, Eq. (7) can be rearranged as

$$\dot{\boldsymbol{X}} = \boldsymbol{h}(\boldsymbol{X}) + \boldsymbol{g}(\boldsymbol{X})W(t) \tag{8}$$

Eq. (8) is called a Langevin equation [4,28,29,31], which takes the physical responses as basic unknowns, and can be rewritten as a SDE in the Itô form [28,31]

$$\mathrm{d}\boldsymbol{X} = \boldsymbol{h}(\boldsymbol{X})\mathrm{d}t + \boldsymbol{g}(\boldsymbol{X})\mathrm{d}W_t(t) \tag{9}$$

in which $W_t(t)$ is a Wiener process [4,28] and

$$\begin{aligned}\boldsymbol{h} &= \left\{\begin{array}{c} X_2 \\ \dfrac{X_2^2 \sin X_1 + s_1 X_2 \sec X_1 + s_2 \tan X_1 + s_3 \sin X_1 + s_4}{(s_5 \sec X_1 - \sin X_1 \tan X_1)} \end{array}\right\} \\ \boldsymbol{g} &= \left\{\begin{array}{c} 0 \\ \dfrac{s_6}{(s_5 \sec X_1 - \sin X_1 \tan X_1)} \end{array}\right\}\end{aligned} \tag{10}$$

where

$$\begin{aligned}&s_1 = \frac{c}{4m_s L^2}, \qquad s_2 = \frac{F_s^0 + 2k_s L\cos\theta_0}{2m_s L}, \qquad s_3 = \frac{k_a - 4k_s}{4m_s} \\ &s_4 = -\frac{2F_s^0 \tan\theta_0 + k_a L \sin\theta_0}{4m_s L}, \qquad s_5 = -\frac{m_a}{4m_s}, \qquad s_6 = -\frac{1}{4m_s L}\end{aligned} \tag{11}$$

2.3 Fokker-Planck equation

FPEs are traditionally derived by extracting the statistical information from the Langevin equations [31,41], and as mentioned before, FPEs govern the evolution process of the physical response PDF over the phase space (denoted by Ω). Eqs. (8) and (9) correspond to the FPE

$$\frac{\partial p_{\boldsymbol{X}}}{\partial t} = Dg_2^2 \frac{\partial^2 p_{\boldsymbol{X}}}{\partial x_2^2} - x_2 \frac{\partial p_{\boldsymbol{X}}}{\partial x_1} - \frac{\partial (h_2 p_{\boldsymbol{X}})}{\partial x_2} \tag{12}$$

where $p_{\boldsymbol{X}} = p_{\boldsymbol{X}}(\boldsymbol{x}, t|\boldsymbol{x}', t')$ is the transition PDF of the state vector $\boldsymbol{X}$. $\boldsymbol{x}$ and $\boldsymbol{x}'$ are the values of $\boldsymbol{X}$ at time t and t', h_2 and g_2 are the second components of $\boldsymbol{h}(\boldsymbol{x})$ and $\boldsymbol{g}(\boldsymbol{x})$, respectively.

From Bayes' theorem, the PDF of $\boldsymbol{X}$ at time t can be expressed as

$$f_{\boldsymbol{X}}(\boldsymbol{x}, t) = \int_{\Omega} p_{\boldsymbol{X}}(\boldsymbol{x}, t|\boldsymbol{x}', t') f_{\boldsymbol{X}}(\boldsymbol{x}', t') \, \mathrm{d}x_1' \mathrm{d}x_2' \tag{13}$$

which is actually a state function. Based on Eqs. (12) and (13), it is easy to show that $f_{\boldsymbol{X}}(\boldsymbol{x}, t)$ also satisfies the FPE (12) [31], i.e.

$$\frac{\partial f_{\boldsymbol{X}}}{\partial t} = Dg_2^2 \frac{\partial^2 f_{\boldsymbol{X}}}{\partial x_2^2} - x_2 \frac{\partial f_{\boldsymbol{X}}}{\partial x_1} - \frac{\partial (h_2 f_{\boldsymbol{X}})}{\partial x_2} \tag{14}$$

with the initial condition

$$f_{\boldsymbol{X}}(\boldsymbol{x}, 0) = \begin{cases} \delta(\boldsymbol{x} - \boldsymbol{x}_0) & \text{deterministic} \\ f_{\boldsymbol{X}}^0(\boldsymbol{x}) & \text{probabilistic} \end{cases} \tag{15}$$

in which $\boldsymbol{x}_0 = (x_{0,1}, x_{0,2})$ is a deterministic initial value, $\delta(\cdot)$ is the Dirac delta function, and $f_{\boldsymbol{X}}^0(\boldsymbol{x})$ is a given initial distribution. In the numerical solution of FPEs, however, a deterministic initial value cannot be simulated precisely and may be approximated by the limit of a Gaussian distribution, i.e.

$$f_{\boldsymbol{X}}(\boldsymbol{x},0)=\lim_{\sigma_1,\sigma_2\to 0}\frac{1}{2\pi\sigma_1\sigma_2}\exp\left\{-\frac{1}{2}\left[\frac{\left(x_1-x_{0,1}\right)^2}{\sigma_1^2}+\frac{\left(x_2-x_{0,2}\right)^2}{\sigma_2^2}\right]\right\} \tag{16}$$

In principle, the boundary conditions of the FPE are $\lim_{x_1,x_2\to\infty} f_{\boldsymbol{X}}(\boldsymbol{x},t)=0$, while in the numerical simulation, the unbounded phase space needs to be truncated and the following Dirichlet boundary conditions are usually adopted

$$f_{\boldsymbol{X}}(\boldsymbol{x},t)|_{x_1=A_1,A_2}=0,\qquad f_{\boldsymbol{X}}(\boldsymbol{x},t)|_{x_2=B_1,B_2}=0 \tag{17}$$

The constants A_1, A_2, B_1 and B_2 should be properly selected to supply a truncated domain such that the PDF values on the boundaries are always almost equal to zero during the realistic evolution process in the unbounded case. Therefore, from an approximation solution point of view, Eq. (17) is able to give a sufficiently precise solution of the PDF evolution process within the truncated domain. In the following, the truncated domain is still denoted by Ω.

3 Evolution process of physical response PDF

3.1 Monte Carlo simulation

The random initial distribution $f_{\boldsymbol{X}}(\boldsymbol{x},0)=f_{\boldsymbol{X}}^0(\boldsymbol{x})$ defined over the phase space Ω can be simulated by a series of discrete samples, and a MCS may be executed sequentially based on Eq. (9). The commonly used uniform-weighted sampling is applied here [42].

The SDE (9) can be numerically solved by stochastic direct integration schemes [4,28], e.g., the Euler-Maruyama scheme which takes the form

$$\boldsymbol{X}^{(k+1)}=\boldsymbol{X}^{(k)}+\boldsymbol{h}\left(\boldsymbol{X}^{(k)}\right)\Delta t+\boldsymbol{g}\left(\boldsymbol{X}^{(k)}\right)\Delta W^{(k)},\qquad k=1,2,3,\ldots \tag{18}$$

where Δt is the step size and $\Delta W^{(k)}$ is a series of independent zero-mean

Gaussian variables with the same variance $2D\Delta t$.

Despite the inherent continuity of the physical response, the sample paths generated by the iteration formula Eq. (18) can be easily converted into an Eulerian framework. Suppose the total number of samples is N_s, giving a fixed mesh $\Omega = \bigcup_{i=1}^{N_x} \Omega_i$ for the truncated domain, where N_x is the total number of elements. If the number of samples located in an element Ω_i at time t_j is n_i, then the probability of the physical response being located in Ω_i can be estimated as

$$P\{\boldsymbol{X}(t_j) \in \Omega_i\} = \frac{n_i}{N_s} \tag{19}$$

Assuming the physical response $\boldsymbol{X}$ follows a uniform distribution on Ω_i, then its PDF obtained by MCS can be expressed as

$$f_{\boldsymbol{X}}(\boldsymbol{x}, t_j) = \frac{P\{\boldsymbol{X}(t_j) \in \Omega_i\}}{S_{\Omega_i}} = \frac{n_i}{N_s S_{\Omega_i}}, \quad \boldsymbol{x} \in \Omega_i \tag{20}$$

where S_{Ω_i} is the area of the element Ω_i. Executing such operations for each element, the physical response PDF over the whole truncated domain Ω at each time t_j can be obtained.

It should be noted that the operations above based on the MCS sample paths only provide a rough approximation of the physical response PDF $f_{\boldsymbol{X}}(\boldsymbol{x}, t)$. However this does not affect the present investigation of the evolution process of $f_{\boldsymbol{X}}(\boldsymbol{x}, t)$ from an overall perspective. Besides, it is easy to deduce that when $N_s \to \infty$, and $S_{\Omega_i} \to 0$ ($N_x \to \infty$), the obtained PDF converges to the precise distribution, which can be obtained in the manner given in the following section.

3.2 Solving FPE by FEM

The FPE (14) can be solved by FDM or FEM [34-36]. The Bubnov-Galerkin

FEM is adopted here, and the mesh is chosen to be the same as in Section 3.1, i.e. $\Omega = \bigcup_{j=1}^{N_x} \Omega_j$.

A piecewise interpolation of the PDF takes the form

$$f_{\boldsymbol{X}}(\boldsymbol{x}) = \bigcup_{j=1}^{N_x} \sum_{i=1}^{M} N_i(\boldsymbol{x}) f_{\boldsymbol{X}_i}^{\ j}(t) \tag{21}$$

where M is the number of shape functions $N_i(\boldsymbol{x})$, i is the node number and j is the element number.

The residual function is

$$\mathcal{R}(\boldsymbol{x}, t) = \frac{\partial f_{\boldsymbol{X}}}{\partial t} - D g_{22}^2 \frac{\partial^2 f_{\boldsymbol{X}}}{\partial x_2^2} + x_2 \frac{\partial f_{\boldsymbol{X}}}{\partial x_1} + h_2 \frac{\partial f_{\boldsymbol{X}}}{\partial x_2} + f_{\boldsymbol{X}} \frac{\partial h_2}{\partial x_2} \tag{22}$$

Taking the shape functions as weight functions

$$\int_{\Omega_j} \mathcal{R}(\boldsymbol{x}, t) N_j(\boldsymbol{x}) \, \mathrm{d}x_1 \mathrm{d}x_2 = 0 \tag{23}$$

Substituting Eqs. (21) and (22) into Eq. (23), and applying integration by parts to the second partial derivative terms gives

$$\boldsymbol{C}\dot{\boldsymbol{f}}_{\boldsymbol{X}} + \boldsymbol{K}\boldsymbol{f}_{\boldsymbol{X}} = \boldsymbol{0} \tag{24}$$

in which the vector $\boldsymbol{f}_{\boldsymbol{X}}$ consists of PDF values on nodes. The elements of the coefficient matrices $\boldsymbol{C}$ and $\boldsymbol{K}$ are

$$\begin{aligned} C_{ij} &= \int_{\Omega_\mathrm{e}} N_i N_j \, \mathrm{d}x_1 \mathrm{d}x_2 \\ K_{ij} &= \int_{\Omega_\mathrm{e}} N_i \left(x_2 \frac{\partial N_j}{\partial x_1} + h_2 \frac{\partial N_j}{\partial x_2} + N_j \frac{\partial h_2}{\partial x_2} \right) + D g_{22}^2 \frac{\partial N_i}{\partial x_2} \frac{\partial N_j}{\partial x_2} \mathrm{d}x_1 \mathrm{d}x_2 \end{aligned} \tag{25}$$

It can be seen that for a group of given shape functions, C_{ij} are constants, while K_{ij} are functions of the vector $\boldsymbol{x}$. Meanwhile, the matrix $\boldsymbol{C}$ is symmetric,

while the matrix $\boldsymbol{K}$ has involved the inhomogeneous drift and diffusion characteristics of the physical response PDF over the phase space, and is generally asymmetric.

Following the general steps of FEM, the matrices are assembled and the Dirichlet boundary conditions of Eq. (17) are applied. Finally, the obtained matrix differential equations can be easily solved by temporal numerical integration methods.

4 Snapping-through and its statistical analysis

In the fatigue life assessment of structures excited by random loads, especially for nonlinear cases, the rainflow counting method [38,39] is usually applied to obtain the number and amplitudes of stress/strain cycles based on pre-acquired stress/strain response sample paths. Combining with Miner's rule and the S-N (stress/strain) curve of the constituent materials, the fatigue life of the structures can be estimated [37-39]. It is obvious that for such engineering assessment procedures and their analogues, a dynamic analysis using Lagrangian-description-based methods must be adopted in advance.

Given the above facts and backgrounds, this section presents a discussion of the statistical regularities of physical quantities for structural assessment under the statistical steady state condition, by counting the number and amplitudes of snapping-through of the bistable SMRSs as a representative example.

Fig. 4 shows a typical physical response sample path of bistable structures, which consists of local vibrations around the stable static equilibrium positions $X_1 = \theta_{s,1}$ and $X_1 = \theta_{s,2}$ (intra-well response) and switching of motion statuses that passes through the potential barrier $X_1 = \theta_0$ (cross-well response).

In order to execute a quantitative analysis, one loop of motion statuses which takes the potential barrier $X_1 = \theta_0$ as the reference position is defined as one snapping-through, as shown in Fig. 4. The maximum absolute distances from the reference position $X_1 = \theta_0$ during local vibrations of the structure, i.e. A^+ and A^- are used to indicate the strength of snapping-through. Meanwhile, the number of snapping-through S over a given time interval $[T_1, T_2]$ is used to indicate the frequency. On the assumption that the local vibration induces negligible structural damage, the aforementioned scheme is quite similar to the handling of stress/strain sample paths in the rainflow counting method, except that it now deals with deformation sample paths, i.e. X_1. This does not affect the essence of the problem.

Based on the deformation sample paths obtained by MCS in Section 3.1, the mean value and variance of S over a given time interval $[T_1, T_2]$ are estimated as

$$\mu_S = \frac{1}{N_s}\sum_{i=1}^{N_s} s_i, \quad \sigma_S^2 = \frac{1}{N_s}\sum_{i=1}^{N_s}(s_i - \mu_S)^2 \tag{26}$$

where s_i is the number of snapping-through of the structure over $[T_1, T_2]$ revealed by sample path i (with probability $1/N_s$). The mean values and variances of A^+ and A^- are estimated as

$$\begin{aligned} \mu_{A^+} &= \frac{1}{N_s}\sum_{i=1}^{N_s}\sum_{j=1}^{s_i}\frac{a_{ij}^+}{s_i}, \quad \sigma_{A^+}^2 = \frac{1}{N_s}\sum_{i=1}^{N_s}\sum_{j=1}^{s_i}\frac{\left(a_{ij}^+ - \mu_{A^+}\right)^2}{s_i} \\ \mu_{A^-} &= \frac{1}{N_s}\sum_{i=1}^{N_s}\sum_{j=1}^{s_i}\frac{a_{ij}^-}{s_i}, \quad \sigma_{A^-}^2 = \frac{1}{N_s}\sum_{i=1}^{N_s}\sum_{j=1}^{s_i}\frac{\left(a_{ij}^- - \mu_{A^-}\right)^2}{s_i} \end{aligned} \tag{27}$$

where a_{ij}^+ and a_{ij}^- are the absolute distances from $X_1 = \theta_0$ during the jth snapping-through of sample path i (with probability $1/N_s s_i$). In general, the statistics in Eqs. (26) and (27) are all related to the start time T_1 and end time T_2

of the given time interval.

Suppose the structure has arrived at the statistical steady state. From a sampling perspective, this means the statistics in Eqs. (26) and (27) are only related to the length of the time interval $\Delta T = T_2 - T_1$, since the PDF of the physical response is now time-independent. The statistics of random variable S over a given time span ΔT are denoted by $\tilde{\mu}_S$ and $\tilde{\sigma}_S^2$. Since the response has the Markovian property [4,28,31], the persistent snapping-through actually consists of a collection of independent repetition events. According to the central-limit theorem, it is easy to deduce that the number of snapping-through R over another arbitrary time span Γ follows the Gaussian distribution with mean value $\tilde{\mu}_S\Gamma/\Delta T$ and variance $\tilde{\sigma}_S^2\Gamma/\Delta T$, i.e.

$$f_R(r) = \frac{1}{\sqrt{2\pi\tilde{\sigma}_S^2\Gamma/\Delta T}} \exp\left[-\frac{(r-\tilde{\mu}_S\Gamma/\Delta T)^2}{2\tilde{\sigma}_S^2\Gamma/\Delta T}\right] \tag{28}$$

where ΔT serves as a reference time span.

Furthermore, it can be seen in Eq. (27) that except for an ensemble averaging, the statistics of A^+ and A^- are obtained simultaneously by a time averaging (through s_i), which is not contained in the definitions of the statistics of S in Eq. (26) where additive operations over time are implied. As has been mentioned before, the persistent snapping-through of the structure consists of independent repetition events, and the physical quantities A^+ and A^- are characteristic physical quantities uniformly defined for every single event. Thus according to the law of large numbers, as time span increases, the statistics of A^+ and A^- tend to be time-independent for the values of A^+ and A^- extracted from the sample paths can be seen as performed trials. Similarly, the statistics in Eq. (27) over a reference time

span ΔT are denoted by $\tilde{\mu}_{A^+}$, $\tilde{\sigma}^2_{A^+}$, $\tilde{\mu}_{A^-}$ and $\tilde{\sigma}^2_{A^-}$.

It should be noted that the reference time span ΔT can be far less than Γ, which means the statistical information of snapping-through under the statistical steady state condition can be completely obtained based on a short-term MCS, as long as the statistical regularities of concerned physical quantities are deduced or detected numerically. The inferences above will be numerically verified in Section 5.2.

5 Numerical examples and discussions

The properties and related parameters of a bistable SMRS are given in Table 1.

The distribution of mechanical energy levels corresponding to different dynamic states of this SMRS over the phase space can be indicated by a selected function $\Pi_{\log}(\boldsymbol{x}) = \log(T + V + 1)$, as shown in Fig. 5.

As can be seen in Fig. 5, two stable static equilibrium positions $\theta_{s,1} = -0.530\text{rad}$ and $\theta_{s,2} = 0.436\text{rad}$ are surrounded by two asymmetric potential wells in the range $\Theta \in (-\pi/2, \pi/2)$, respectively. Consequently, the response of the structure is determined by the attracting effects of these two areas on both sides of the potential barrier $\theta_0 = 0.1\text{rad}$, together with the external excitations.

5.1 Comparison of methods

The solution domain is uniformly set as a truncated rectangle $\Omega = \{(x_1, x_2) | -2 \le x_1 \le 2, -5 \le x_2 \le 5\}$ of the phase space, with 100×250 uniform and fixed elements. The Euler-Maruyama algorithm is adopted for the

MCS, and the fourth-order Runge-Kutta algorithm is adopted for the FPE analysis, with the same step size $\Delta t = 0.002$s. Bilinear elements are adopted in the FEM.

Suppose the initial state of the structure follows a 2D Gaussian distribution with mean values $(0.5,0.5)$ and variances $(0.0625,0.0625)$. Applying the MCS and FPE to analyze the evolution process of the physical response PDF, results during 0~5s are shown in Fig. 6.

It can be seen that overall equivalent PDF evolution processes have been obtained by the two methods except for certain differences of resolution. As the number of sample paths is increased, the details of the results obtained by MCS are more distinct and are closer to the results obtained by FPE.

For a fixed mesh, the PDF evolution process is indeed indicated by the variation of PDF values on nodes over time. Extracting PDF vectors every 1s (500 steps) to constitute a new sequence, and adopting the Frobenius norm $\eta_F^{(k+1)} = \left\| \left[\boldsymbol{f}_{\boldsymbol{X}}^{(k+1)} \right] - \left[\boldsymbol{f}_{\boldsymbol{X}}^{(k)} \right] \right\|_F, (k = 0,1,2,\dots)$ with $\left[\boldsymbol{f}_{\boldsymbol{X}}^{(k)} \right]$ the PDF vector at $t = k$s, the convergence process of the physical response PDF is shown as in Fig. 7.

Fig. 7 indicates that from a given initial distribution, the physical response PDF of the structure tends to be time-independent. It can also be seen that MCS with less sample paths exhibits larger fluctuations of convergence level, which is mainly due to the rough transformation of the Lagrangian-description-based physical response sample paths to the Eulerian-description-based PDF according to Eq. (20), and this can also be improved by increasing the number of sample paths. The FPE analysis shows an elegant convergence behavior. In practice, the physical quantity η_F can be used to judge the existence and the arrival time of a statistical steady state in engineering applications, since in general these cannot be explicitly

deduced in advance mathematically [29,43,44]. In addition, it should be noted that a statistical steady state approximates the steady state solution of the corresponding FPE, with terms involve time being zero, and is indeed not related to the initial state of structures.

According to Fig. 7, taking $t = 40$s as the time instant when the structure arrives at the statistical steady state, the corresponding physical response PDF obtained by FPE and MCS are given in Fig. 8.

It can also be seen that results obtained by MCS with more samples show more consistency in details with the results given by FPE.

From a more comprehensive perspective, in principle, the amount of essential statistical information implied in the random physical response is fixed, and is certainly not related to which method is adopted to obtain it. From an applications perspective, numerical solution of FPE suffers from numerical stability problems which may occur with a coarse mesh or a large step size. Specifically, a coarse mesh may incur poor, or even improper negative approximations to the PDF (which is clearly nonnegative), and the maximum time step size for maintaining global stability for all nodes simultaneously in solving FPE is usually much less than that for only a single sample path in MCS. Consequently, FPE is thought to be inapplicable to the dynamic analysis of multi-degree-of-freedom structures for the curse of dimensionality [34-36] would arise and cannot be alleviated by using coarser meshes or larger step sizes. In MCS, fewer samples may be used to ensure its feasibility, although a low accuracy may be obtained. Meanwhile, the efficiency of MCS can be drastically improved by utilizing parallel computation technologies, as can be revealed by the total computation time listed in Table 2 for the present calculations.

5.2 Statistics of snapping-through

In Section 4, the statistical regularities of the number S and the amplitudes A^+ and A^- of snapping-through of the SMRS have been deduced. For further numerical verifications, MCS with 5×10^4 samples is continued after the time instant t=40s, and a time shifting $\tau = t - 40\text{s}$ is employed.

The variations of the statistics of S, A^+ and A^- with respect to the time τ are obtained as in Fig. 9, where the variances $\sigma_{A^+}^2$ and $\sigma_{A^-}^2$ are multiplied by 10 for ease of presentation.

It should be noted that in Section 4, a snapping-through was defined to start from a specific position $X_1 = \theta_0$. At a given time instant, the samples would not synchronously locate at this position, and so the parts of a sample path before the sample initially arrives, and after the sample finally arrives at $X_1 = \theta_0$ are omitted in the counting algorithm. These operations certainly result in errors of the statistics, as shown in the time ranges $\tau \in [0,40]$s in Fig. 9(a) and $\tau \in [0,150]$s in Fig. 9(b). With the increasing of the time span, the essential statistical regularities of the statistics are revealed as in the latter parts of Figs. 9(a) and Fig. 9(b), where it can be seen that μ_S and σ_S^2 tend to be proportional to the time τ, while μ_{A^+}, $\sigma_{A^+}^2$, μ_{A^-} and $\sigma_{A^-}^2$ are finally time-independent, confirming the deductions in Section 4.

As has been stated in Section 4, according to Fig. 9, taking the reference time span as $\Delta T = 200\,\text{s}$ gives $\tilde{\mu}_S = 27.75$, $\tilde{\sigma}_S^2 = 67.34$, $\tilde{\mu}_{A^+} = 0.6743$, $\tilde{\sigma}_{A^+}^2 = 0.0206$, $\tilde{\mu}_{A^-} = 0.9838$ and $\tilde{\sigma}_{A^-}^2 = 0.0186$. Then comparisons of statistics over a collection of far longer time spans $\Gamma = [2000,4000,6000,8000]$s, deduced by the aforementioned statistical regularities as in Section 4 and obtained by full-time

MCS with 5×10^4 samples, are shown in Fig. 10 and listed in Table 3.

It can be seen in Fig. 10 that the deduced PDF of the number of snapping-through in time span $\Gamma(\Gamma \gg \Delta T)$ as in Eq. (28) is quite consistent with which obtained by full-time MCS. The comparison of statistics of the amplitudes of snapping-through is listed in Table 3, in which it can also be seen that a short-term MCS (ΔT =200s) is able to present quite accurate statistics.

On the other hand, small errors still exist. It is observed in Fig. 10 that the deduced PDF has an overall shifting to the left with respect to that obtained by full-time MCS, and in Table 3, the deduced statistics have relative errors within 2%. Certainly, these errors are insignificant, but it is necessary to state that they can be further reduced by increasing the reference time span. This mainly depends on the specific requirements on accuracy in practical analysis or assessment.

The total computation time for the present calculations is also listed in Table 3 as a reference. The time needed for the calculation of the transient process before t=40s and post-processing of the samples has been included.

As a result, it is summarized that the number and amplitudes of snapping-through of the SMRS have certain statistical regularities that can be deduced or numerically detected. A generalization of this idea means that once a statistical steady state is arrived, using a short-term MCS as a reference may provide sufficient accurate statistical information for the assessment of structures.

6 Conclusions

Some issues involving the stochastic dynamics of bistable structures are investigated in this paper through a simple spring-mass-rod structure (SMRS), by virtue of the essential equivalence in the mechanical characteristics between

SMRSs and general engineering components. Investigations of the bistable mechanisms suggest that both the curvature of a structure itself and buckling can render it to be bistable.

To reveal the capabilities of two commonly used kinds of methodologies for stochastic dynamic analysis of bistable structures, a complete Monte Carlo simulation (MCS) using ensemble averaging within a Lagrangian framework and a Fokker-Planck equation (FPE) analysis using the finite element method within an Eulerian framework are taken as typical feasible procedures to capture the evolution process of physical response probability density function (PDF) of a SMRS. Overall coincident results are given by these two approaches except that the resolution of MCS needs to be improved by increasing the number of samples. Extended discussions from an applications perspective state that the numerical stability problems that may happen in FPE analysis have prohibited the possibility of using a coarse mesh or a large time step size to alleviate the curse of dimensionality in stochastic dynamic analysis of multi-degree-of-freedom structures, while MCS still works in such situations and its efficiency can be further improved by parallel computation, which consequently makes it possible to improve the accuracy with more samples.

It is also noted that since the inherent continuity of physical response is neglected in a FPE analysis, it cannot be used in a structural assessment based on physical response processes such as fatigue life prediction. Subsequently, in view of the movement characteristics of bistable structures, the statistical regularities of the number and amplitudes of snapping-through of the structure under a statistical steady state are deduced and numerically verified. Numerical results also reveal that such statistical regularities can be utilized to dramatically reduce the efforts of

structural assessment without loss of precision.

Acknowledgments

The authors are grateful for support under grants from the National Science Foundation of China (11672060) and the Cardiff University Advanced Chinese Engineering Centre.

Conflict of Interest

The authors declare that they have no conflict of interest.

References

[1] Prengel F, Wacker A, Schöll E. Simple model for multistability and domain formation in semiconductor superlattices. Physical Review B, 1994, 50(3): 1705-1712

[2] Laplante JP, Erneux T. Propagation failure and multiple steady states in an array of diffusion coupled flow reactors. Physica A: Statistical Mechanics and Its Applications, 1992, 188(1-3): 89-98

[3] Seung HS. Continuous attractors and oculomotor control. Neural Networks, 1998, 11(7-8): 1253-1258

[4] Van Kampen NG. Stochastic Processes in Physics and Chemistry. Elsevier, Amsterdam, 1992

[5] Lee HP, Harris PJ. Post-buckling strength of thin-walled members. Computers and Structures, 1979, 10(4): 689-702

[6] Chen NZ, Soares CG. Reliability assessment of post-buckling compressive strength of laminated composite plates and stiffened panels under axial compression. International Journal of Solids and Structures, 2007, 44(22-23): 7167-7182

[7] Falzon BG, Aliabadi MH. Buckling and Post Buckling Structures: Experimental, Analytical and Numerical Studies. Imperial College Press, London, 2008

[8] Dhainaut JM, Guo X, Mei C, Spottswood SM, Wolfe HF. Nonlinear random response of panels in an elevated thermal-acoustic environment. Journal of Aircraft, 2003, 40(4): 683-691

[9] Chen H, Virgin LN. Finite element analysis of post-buckling dynamics in plates. Part I: An asymptotic approach. International Journal of Solids and Structures, 2006, 43(13): 3983-4007

[10] Chen H, Virgin LN. Finite element analysis of post-buckling dynamics in plates. Part II: A non-stationary analysis. International Journal of Solids and Structures, 2006, 43(13): 4008-4027

[11] Liu L, Lv B, He T. The stochastic dynamic snap-through response of thermally buckled

composite panels. Composite Structures, 2015, 131: 344-355

[12] Miller BA, McNamara JJ, Spottswood SM, Culler AJ. The impact of flow induced loads on snap-through behavior of acoustically excited, thermally buckled panels. Journal of Sound and Vibration, 2011, 330(23): 5736-5752

[13] Chen JS, Lin JS. Dynamic snap-through of a shallow arch under a moving point load. Journal of Vibration and Acoustics, Transactions of ASME, 2004, 126(4): 514-519

[14] Cottone F, Vocca H, Gammaitoni L. Nonlinear energy harvesting. Physical Review Letters, 2009, 102(8): 080601

[15] Tang L, Yang Y, Soh CK. Toward broadband vibration-based energy harvesting. Journal of Intelligent Material Systems and Structures, 2010, 21(18): 1867-1897

[16] Kim HS, Kim JH, Kim J. A review of piezoelectric energy harvesting based on vibration. International Journal of Precision Engineering and Manufacturing, 2011, 12(6): 1129-1141

[17] Daqaq MF, Masana R, Erturk A, Quinn DD. On the role of nonlinearities in vibratory energy harvesting: a critical review and discussion. Applied Mechanics Reviews, 2014, 66(4): 040801

[18] Daqaq MF. Transduction of a bistable inductive generator driven by white and exponentially correlated Gaussian noise. Journal of Sound and Vibration, 2011, 330(11): 2554-2564

[19] Kumar P, Narayanan S, Adhikari S, Friswell MI. Fokker-Planck equation analysis of randomly excited nonlinear energy harvester. Journal of Sound and Vibration, 2014, 333(7): 2040-2053

[20] Cherkaev A, Cherkaev E, Slepyan L. Transition waves in bistable structures. I. Delocalization of damage. Journal of the Mechanics and Physics of Solids, 2005, 53(2): 383-405

[21] Slepyan L, Cherkaev A, Cherkaev E. Transition waves in bistable structures. II. Analytical solution: wave speed and energy dissipation. Journal of the Mechanics and Physics of Solids, 2005, 53(2): 407-36

[22] Nadkarni N, Daraio C, Kochmann DM. Dynamics of periodic mechanical structures containing bistable elastic elements: From elastic to solitary wave propagation. Physical Review E, 2014, 90(2): 023204

[23] Nadkarni N, Arrieta AF, Chong C, Kochmann DM, Daraio C. Unidirectional transition waves in bistable lattices. Physical Review Letters, 2016, 116(24): 244501

[24] Schultz MR. A concept for airfoil-like active bistable twisting structures. Journal of Intelligent Material Systems and Structures, 2008, 19(2): 157-169

[25] Kuder IK, Arrieta AF, Raither WE, Ermanni P. Variable stiffness material and structural concepts for morphing applications. Progress in Aerospace Sciences, 2013, 63: 33-55

[26] Lachenal X, Daynes S, Weaver PM. Review of morphing concepts and materials for wind turbine blade applications. Wind Energy, 2013, 16(2): 283-307

[27] Hu N, Burgueño R. Buckling-induced smart applications: recent advances and trends. Smart

Materials and Structures, 2015, 24(6): 063001

[28] Kloeden PE, Platen E. Numerical Solution of Stochastic Differential Equations. Springer, Berlin, 1999

[29] Soong TT. Random Differential Equations in Science and Engineering. Elsevier, New York, 1973

[30] Cho H. High-Dimensional Response-Excitation PDF Methods for Uncertainty Quantification and Stochastic Modeling. Doctoral dissertation, Brown University, 2015

[31] Risken H. The Fokker-Planck Equation: Methods of Solution and Applications. Springer, Berlin, 1989

[32] Eckmann JP, Ruelle D. Ergodic theory of chaos and strange attractors. Reviews of Modern Physics, 1985, 57(3): 617-656

[33] Walters P. An Introduction to Ergodic Theory. Springer, New York, 2000

[34] Spencer BF Jr, Bergman LA. On the numerical solution of the Fokker-Planck equation for nonlinear stochastic systems. Nonlinear Dynamics, 1993, 4(4): 357-372

[35] Floris C. Numeric solution of the Fokker-Planck-Kolmogorov equation. Engineering, 2013, 5(12): 975-988

[36] Masud A, Bergman LA. Solution of the four dimensional Fokker-Planck equation: still a challenge. In: Augusti G, Schuëller GI, Ciampoli M (Eds.), Proceedings of ICOSSAR 2005, Millpress Science Publishers, Rotterdam, 2005, pp. 1911-1916

[37] Suresh S. Fatigue of Materials. Cambridge University Press, Cambridge, 1998

[38] Wirsching PH, Shehata AM. Fatigue under wide band random stresses using the rain-flow method. Journal of Engineering Materials and Technology, Transactions of ASME, 1977, 99(3): 205-211

[39] Dirlik T. Application of computers in fatigue analysis. Doctoral dissertation, University of Warwick, 1985

[40] Waite JJ, Virgin LN, Wiebe R. Competing responses in a discrete mechanical system. International Journal of Bifurcation and Chaos, 2014, 24(1): 1430003

[41] Caughey TK. Derivation and application of the Fokker-Planck equation to discrete nonlinear dynamic systems subjected to white random excitation. Journal of the Acoustical Society of America. 1963, 35(11): 1683-1692

[42] Avellaneda M, Buff R, Friedman C, Grandechamp N, Kruk L, Newman J. Weighted Monte Carlo: a new technique for calibrating asset-pricing models. International Journal of Theoretical and Applied Finance, 2001, 4(1): 91-119

[43] Huang W, Ji M, Liu Z, Yi Y. Steady states of Fokker-Planck equations: I. Existence. Journal of Dynamics and Differential Equations, 2015, 27(3-4): 721-742

[44] Huang W, Ji M, Liu Z, Yi Y. Steady states of Fokker-Planck equations: II. Non-existence. Journal of Dynamics and Differential Equations, 2015, 27(3-4): 743-762

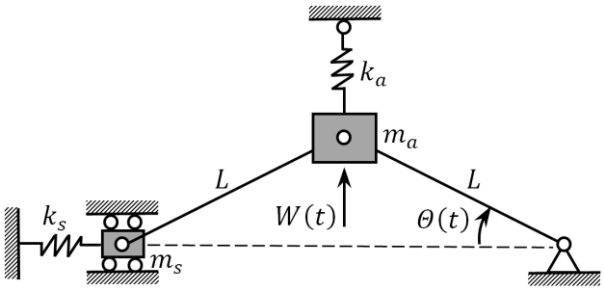

Fig. 1 A single-degree-of-freedom SMRS

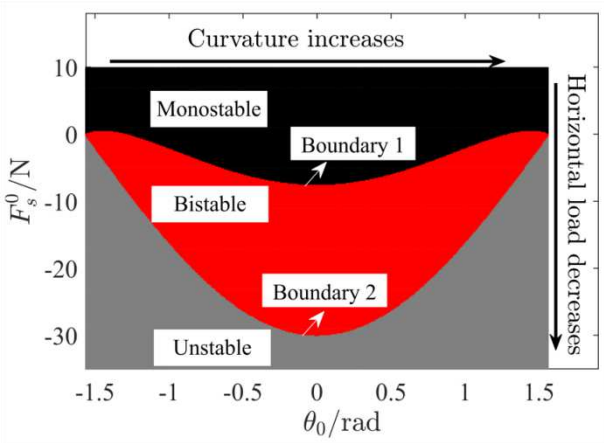

(a) Distribution of monostability and bistability over the parameter space F_s^0-θ_0

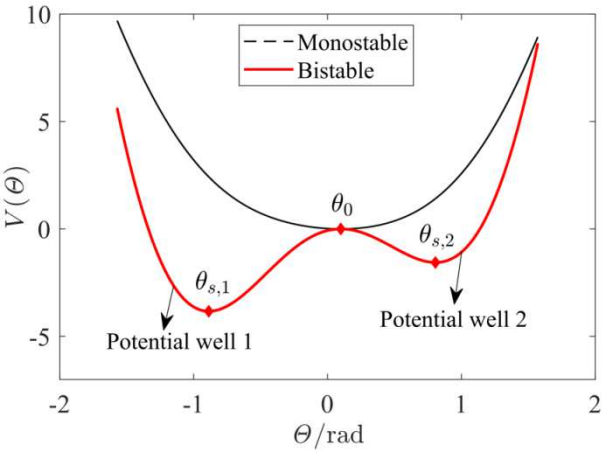

(b) Typical elastic potential energy function of monostable and bistable structures

Fig. 2 Monostability and bistability of the SMRS

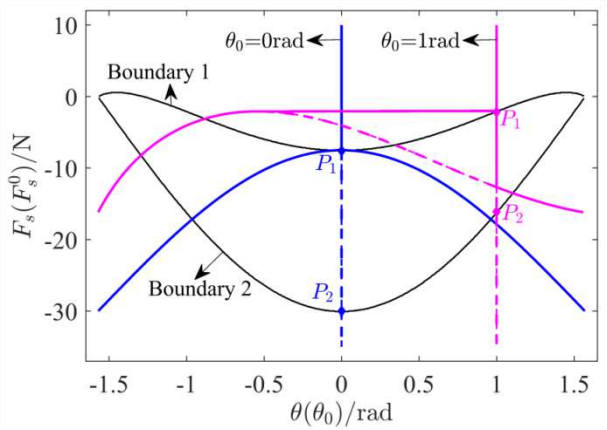

Fig. 3 Nonlinear buckling paths of SMRSs

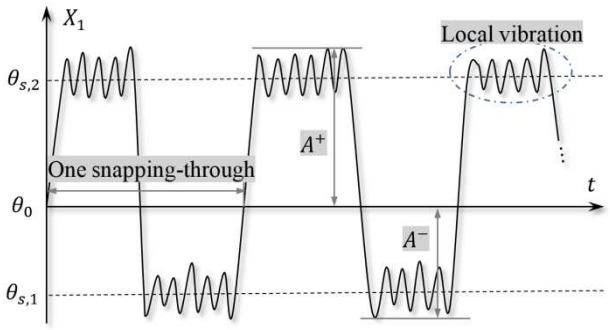

Fig. 4 Schematic of snapping-through of bistable structures

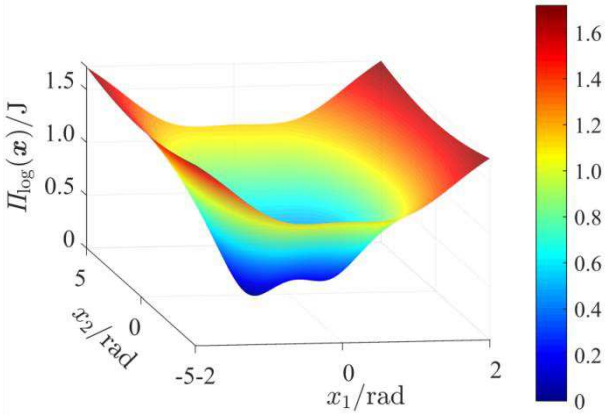

Fig. 5 Mechanical energy distribution over the phase space

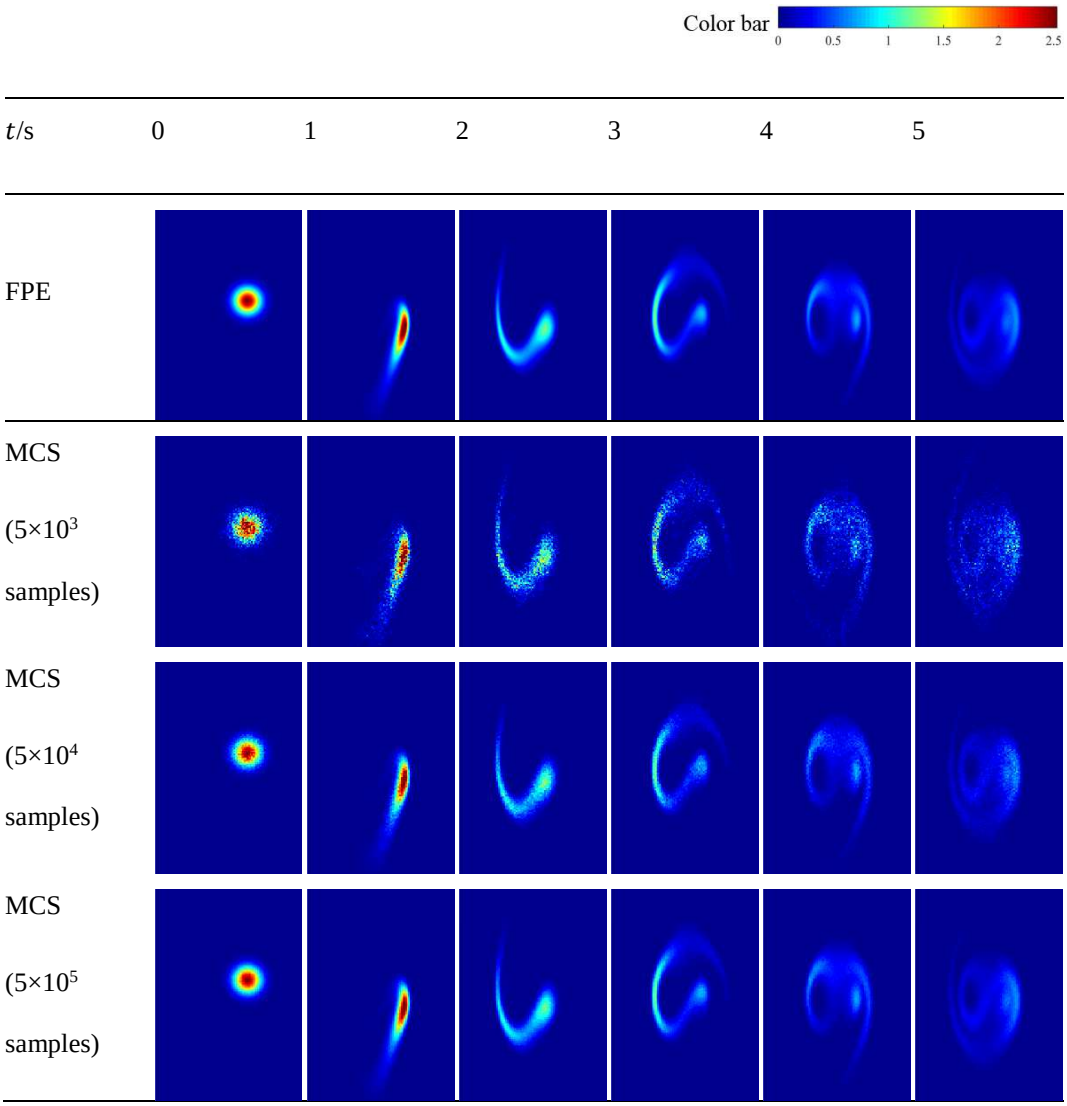

Note: for ease of presentation, the results are further truncated in the range $\{(x_1, x_2)| -1.5 \leq x_1 \leq 1.5, -3 \leq x_2 \leq 3\}$.

Fig. 6 Evolution process of the physical response PDF

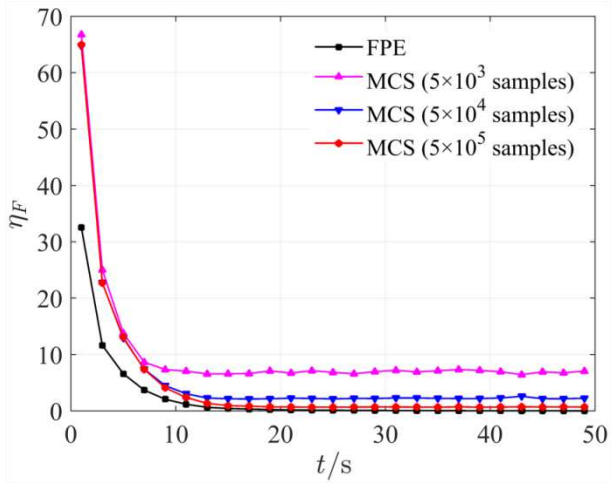

Fig. 7 Convergence process of the physical response PDF

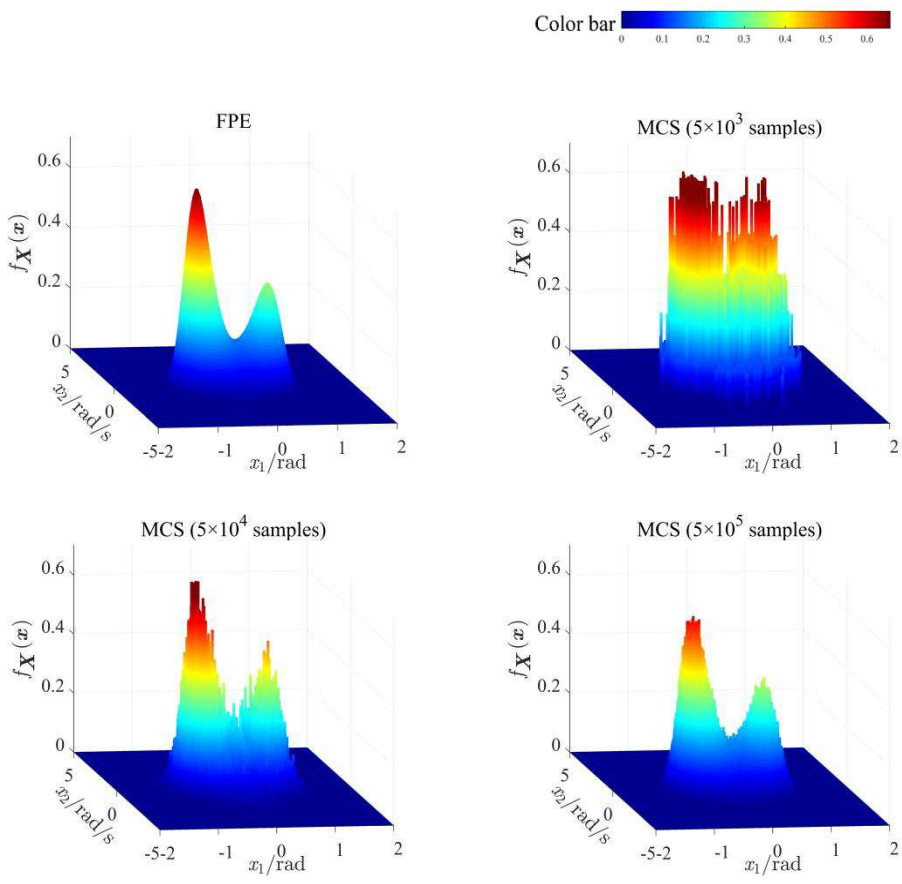

Fig. 8 Physical response PDF in the statistical steady state

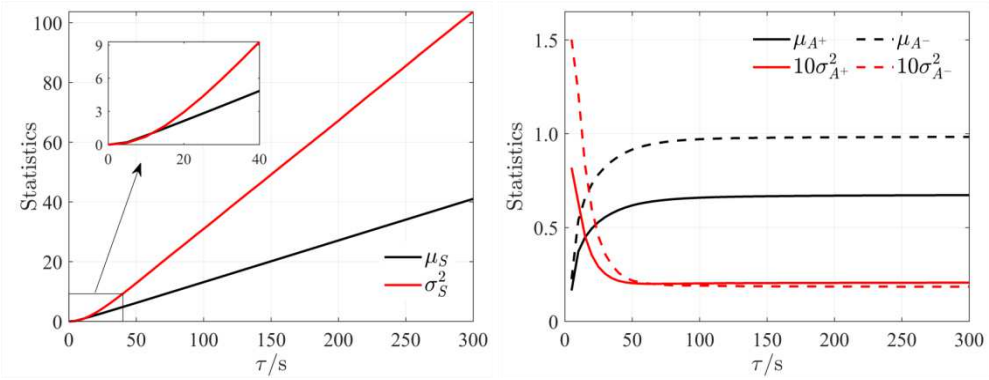

(a) Mean and variance of S (b) Mean and variance of A^+ and A^-

Fig. 9 Variation of statistics with respect to time

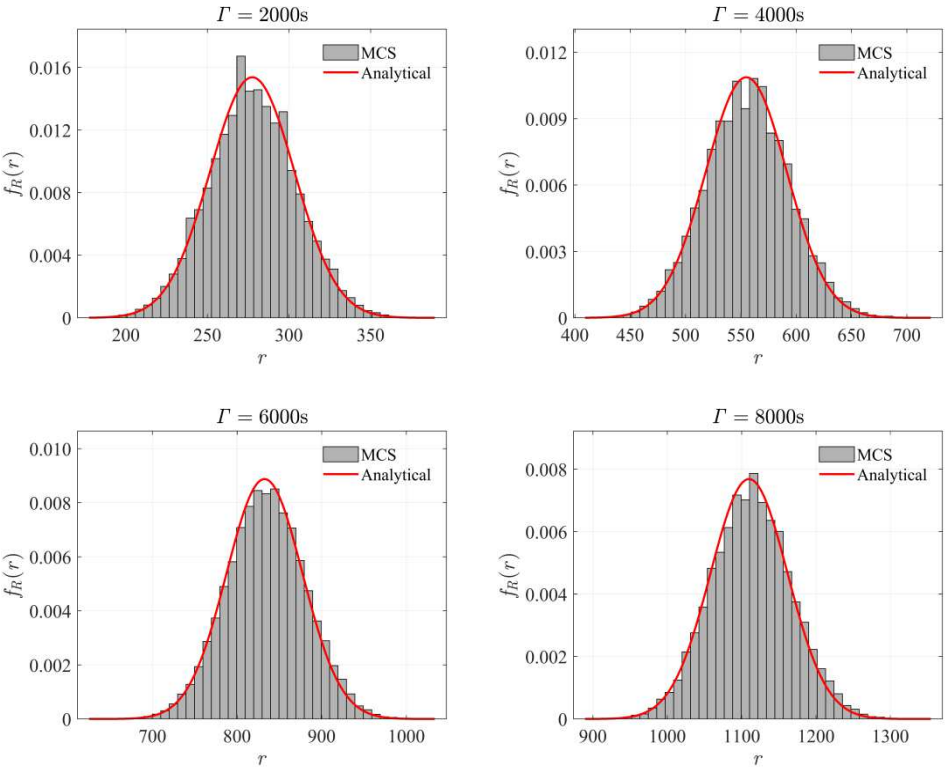

Fig. 10 Comparison of PDFs of the number of snapping-through over given time spans obtained by deduced analytical expressions and full-time MCS

Table 1 Properties and parameters of a bistable SMRS

Quantity	Physical meaning	Value
m_a	Vertical mass	1kg
m_s	Horizontal mass	1kg
k_a	Vertical stiffness	15N/m
k_s	Horizontal stiffness	15N/m
L	Length of rods	1m
c	Viscous damping coefficient	0.1N·s/m
F_s^0	Restoring force in spring k_s	-10N
$2D$	Variance of white noise	$0.2N^2$
θ_0	Given static equilibrium position	0.1rad

Table 2 Total CPU time needed to obtain the evolution process of PDF during 0~40s

Method	FPE	MCS (5×10^3 samples)	MCS (5×10^4 samples)	MCS (5×10^5 samples)
CPU time/s	80055.5	612.3	6151.6	61697.2

Note: The algorithms are programmed in Matlab, run on a workstation with Intel Xeon E5-2687W v4 (3.00GHz) CPU, Win7 64-bit OS, and 48 workers in MCS, while the FPE analysis is indeed single-threaded.

Table 3 Statistics of the amplitudes of snapping-through over different time spans

Γ/s Statistics	2000	4000	6000	8000	ΔT =200 (Reference)
μ_{A^+}	0.6789	0.6794	0.6795	0.6796	0.6743 (-0.78%)
$\sigma^2_{A^+}$	0.0210	0.0210	0.0210	0.0210	0.0206 (-1.90%)
μ_{A^-}	0.9878	0.9881	0.9883	0.9883	0.9838 (-0.46%)
$\sigma^2_{A^-}$	0.0184	0.0184	0.0184	0.0184	0.0186 (+1.09%)
CPU time/s	320006.2	633612.3	969426.9	1287398.9	36909.6

Note: The algorithms are programmed in Matlab, run on a workstation with Intel Xeon E5-2687W v4 (3.00GHz) CPU and 48 workers, Win7 64-bit OS.